# Experimental Realization of Geometry-Dependent Skin Effect in a Reciprocal Two-Dimensional Lattice

Wei Wang,[2,*] Mengying Hu,[1,*] Xulong Wang,[2] Guancong Ma,[2] and Kun Ding[1]
[1]Department of Physics, State Key Laboratory of Surface Physics, and Key Laboratory of Micro and Nano Photonic Structures (Ministry of Education), Fudan University, Shanghai 200438, China
[2]Department of Physics, Hong Kong Baptist University, Kowloon Tong, Hong Kong, China

(Received 9 February 2023; revised 4 August 2023; accepted 17 October 2023; published 15 November 2023)

Recent studies of non-Hermitian periodic lattices unveiled the non-Hermitian skin effect (NHSE), in which the bulk modes under the periodic boundary conditions (PBC) become skin modes under open boundary conditions. The NHSE is a topological effect owing to the nontrivial spectral winding, and such spectral behaviors appear naturally in nonreciprocal systems. Hence prevailing approaches rely on nonreciprocity to achieve the NHSE. Here, we report the experimental realization of the geometry-dependent skin effect in a two-dimensional reciprocal system, in which the skin effect occurs only at boundaries whose macroscopic symmetry mismatches with the lattice symmetry. The role of spectral reciprocity and symmetry is revealed by connecting reflective channels at given boundaries with the spectral topology of the PBC spectrum. Our work highlights the vital role of reciprocity, symmetry, and macroscopic geometry on the NHSE in dimensionality larger than one and opens new routes for wave structuring using non-Hermitian effects.

DOI: 10.1103/PhysRevLett.131.207201

*Introduction.*—The non-Hermitian degrees of freedom [1,2] have broadened the context of the Hamiltonian because, unlike Hermitian Hamiltonians that only treat closed systems with steady states, non-Hermitian Hamiltonians handle open systems [3–5]. Such a generalization necessitates reexamining the basic concepts and relations built on the Hermitian formalism, such as the bulk-edge correspondence [6,7] and spectral degeneracy [8,9]. A significant difference is that the non-Hermitian spectrum lies in the complex plane, resulting in spectral loops and point gaps [10–13], as well as defective spectral degeneracies [14–20]. The research into these unique characteristics has uncovered a plethora of unique phenomena [5,21–23]. Perhaps one of the most prominent phenomena is the non-Hermitian skin effect (NHSE), which causes the bulk modes to collapse towards the open boundary of the system [24–29]. NHSE was discovered by studying one-dimensional (1D) nonreciprocal lattices, wherein the Bloch Hamiltonian has a nonreciprocal spectrum, i.e., $\omega(k) \neq \omega(-k)$ [24,25,30]. It has been confirmed by various experiments in 1D and 2D systems [31–36].

Recent studies further show that NHSE can be enriched by the consideration of symmetry. For example, anomalous time-reversal symmetry can lead to the $\mathbb{Z}_2$ skin effect in one-dimensional lattices [28,37], for which the spectrum under the periodic boundary condition (PBC) is reciprocal, i.e., $\omega(k) = \omega(-k)$. This new classification suggests that nonreciprocal or directional hopping is not always necessary for the NHSE. Extending to 2D systems, it is claimed that the NHSE can universally appear in both nonreciprocal and reciprocal systems [38,39]. Unlike the NHSE in nonreciprocal systems, the combination of the lattice symmetry and spectral reciprocity leads to skin modes localized at generic boundaries but disappear at boundaries matching the line symmetries of the unit cell, i.e., the skin effect is dependent on the geometry of the open-boundary lattice [38,40]. Such geometry-dependent skin effect (GDSE) expands the categories and scenarios of the NHSE in dimensionality larger than one. It also highlights the critical roles of lattice symmetry and macroscopic geometry, which have been largely overlooked in the nonreciprocal NHSE. However, the experimental confirmation of this GDSE so far remains absent.

In this work, we study a 2D model respecting Lorentz reciprocity and displaying a reciprocal complex spectrum, wherein the only form of non-Hermiticity is the onsite gain and loss. By establishing a connection between the geometry of the open boundary and the winding behavior of the PBC spectrum, we identify that the skin effect in such a system only occurs at boundaries that are not parallel to the primitive vectors of the lattice. Such skin effects and the geometry-dependent characteristic are experimentally realized using active mechanical lattices.

*Theoretical model.*—To elucidate the 2D GDSE, we first recall the physics of the nonreciprocal NHSE in 1D open lattices. The PBC spectrum, denoted $\omega^P(k)$, is a complex function that maps the Brillouin zone (BZ) to a closed loop in the 2D complex energy manifold. When such spectral loops enclose a nonzero area, the wave vectors $k$ and $-k$ are mapped to different complex energy. This has profound

 

consequences when the open boundary condition (OBC) is considered: when a wave with a wave vector $k$ impinges on an open boundary, there is no reflective channel with the wave vector $-k$ at the same energy. As a result, the energy carried by the incident wave has no choice other than accumulating at the boundary, leading to the NHSE. On the other hand, if the area enclosed by the spectrum is zero, i.e., the spectral loop collapses to an arc, implying at any complex energy, there exist two choices of wave vectors, and the NHSE does not emerge. Hence, the winding behavior of $\omega^P(k)$ is a convenient tool for predicting the NHSE: a spectral loop (arc) in $\omega^P(k)$, which has a nonzero (zero) winding number, directly corresponds to the occurrence (absence) of the NHSE.

We next consider 2D non-Hermitian lattices. Intuitively, one would expect the skin effect to meet a more stringent set of conditions because there is simply "more room" for the waves to move around, or more channels to leave a boundary. Counterintuitively, the NHSE is ubiquitous and emerges even in the absence of nonreciprocity [38]. To understand this, we consider a stacked non-Hermitian Su-Schrieffer-Heeger model shown in Fig. 1(a). The momentum-space Hamiltonian under the PBC reads

$$H(k_x,k_y)=2\pi\begin{pmatrix} f_A-i\gamma_A+2v_x\cos k_x & v_y+w_y e^{-ik_y} \\ v_y+w_y e^{ik_y} & f_B+i\gamma_B+2v_x\cos k_x \end{pmatrix}, \tag{1}$$

wherein all parameters in Eq. (1) are real. $v_y$ ($w_y$) is the intracell (intercell) hopping in the $y$ direction, and $v_x$ is the hopping along the $x$ direction. The non-Hermiticity is due to $-i\gamma_A$ and $i\gamma_B$, which are the typical onsite loss and gain. Model (1) respects reciprocity because it clearly satisfies $H(k_x,k_y)=H^T(-k_x,-k_y)$. The PBC spectrum is obviously reciprocal, i.e., $\omega^P(k_x,k_y)=\omega^P(-k_x,-k_y)$ [Fig. 1(b)]. Note that model (1) is also Lorentz reciprocal because there is no asymmetric hopping or magnetic flux. In addition, it is easy to check that the spectrum is symmetric in both $k_x$ and $k_y$, i.e., $\omega^P(k_x,k_y)=\omega^P(-k_x,k_y)=\omega^P(k_x,-k_y)$, as shown in Fig. 1(b). These restrictions imply the formation of standing waves, thus the NHSE should be absent. Such conjecture was confirmed in a rectangular lattice, as shown in Fig. 1(c). The color plot depicts the sum of all eigenstates, i.e., $\Psi(\mathbf{x})=(1/N)\sum_n|\psi_n(\mathbf{x})|^2$, where $\psi_n(\mathbf{x})$ is the $n$ th normalized right eigenstate. However, this is not the case if the shape of the OBC lattice is a trapezoid. In Fig. 1(d), one can clearly identify the NHSE at the slanted edge. This is the GDSE.

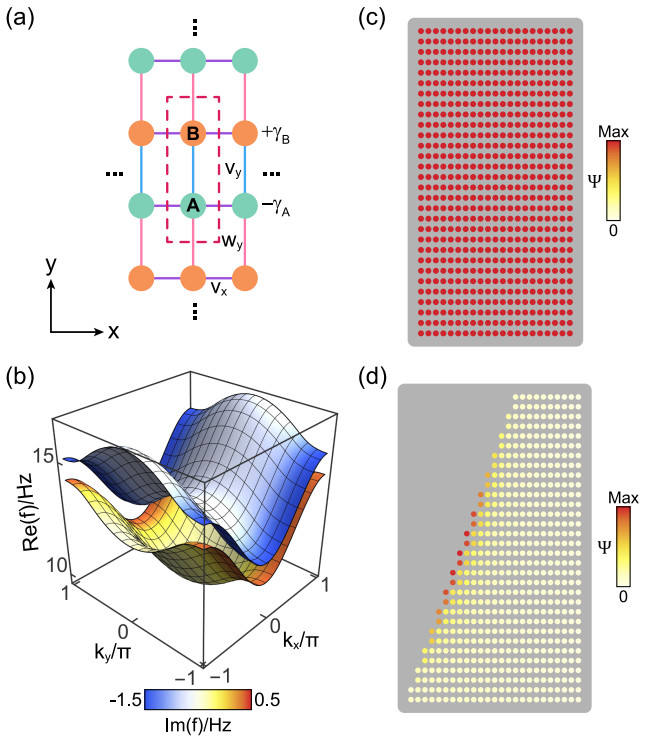


FIG. 1. (a) The 2D non-Hermitian lattice. The dashed box marks the unit cell. (b) The real parts (surfaces) and imaginary parts (color maps) of the PBC spectrum ($\omega^P/2\pi$, unit in Hz). (c),(d) The spatial distribution of $\Psi(\mathbf{x})$ of (c) a rectangular lattice and (d) a trapezoidal lattice.

To gain a comprehensive understanding of the GDSE, we consider the case shown in Fig. 2(a): an incident wave with a wave vector $\boldsymbol{q}^{\mathbf{in}}(\omega)=(q_{\parallel}^{\mathrm{in}},q_{\perp}^{\mathrm{in}})^T$ encounters the slanted open boundary, where $q_{\parallel}^{\mathrm{in}}$ and $q_{\perp}^{\mathrm{in}}$ are the wave vector components parallel and perpendicular to the boundary, respectively. The reflected channels $\boldsymbol{q}^{\mathbf{re}}(\omega)=(q_{\parallel}^{\mathrm{re}},q_{\perp}^{\mathrm{re}})^T=(q_{\parallel}^{\mathrm{in}},q_{\perp}^{\mathrm{re}})^T$ at the same $\omega$ determines whether the NHSE can occur at that boundary. (Here $q_{\parallel}$ is the same for the incident and reflected waves. In other words, the parallel wave vector generated by the boundary is negligible.) The boundary orientation determines the local coordinate of $(\hat{q}_{\parallel},\hat{q}_{\perp})$ in the momentum space, which is linked to $(\hat{k}_x,\hat{k}_y)$ by a frame rotation [Fig. 2(b)]. In other words, the boundary orientation fixes the slope of a series of lines crossing the BZ, such as the red dashed lines in Fig. 2(b). Each line in the $\hat{q}_{\perp}$ direction is a closed parametric loop in the momentum space, and they are mapped to the PBC spectrum as loops by the function $\omega^P(q_{\parallel},q_{\perp})$. The behavior of these spectral loops can be quantified by a spectral winding number

$$\mathcal{W}_{q_{\parallel}}\equiv\frac{1}{2\pi i}\int_{\Gamma_{q_{\parallel}}}\mathrm{d}q_{\perp}(\partial_{q_{\perp}}\ln\det[H(q_{\parallel},q_{\perp})-\omega_b]), \tag{2}$$

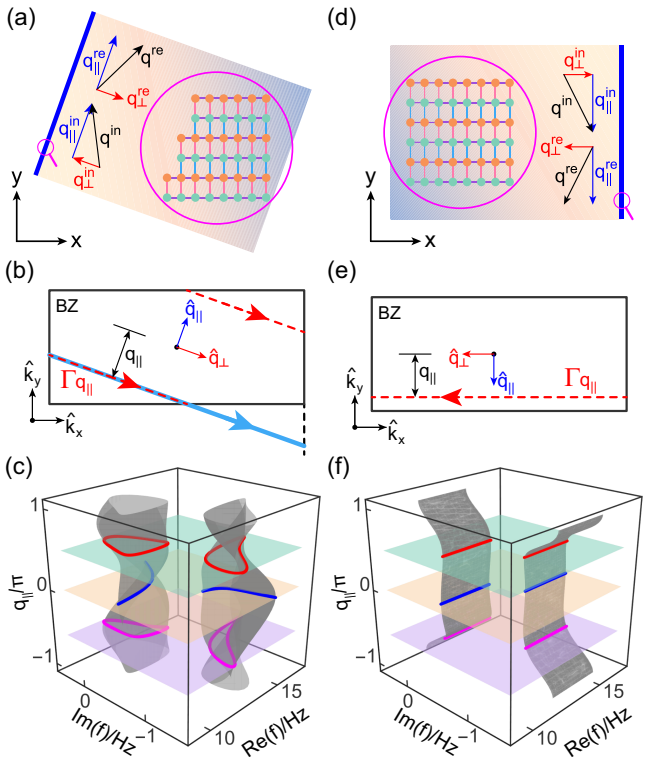


FIG. 2. The schematic of the reflection at (a) a slanted edge and (d) a vertical boundary. The magenta circles show the zoomed-in views of the lattice arrangement at the boundaries. $\Gamma_{q_\parallel}$ with a fixed $q_\parallel$ across the BZ for (b) the slanted edge and (e) the boundary parallel to the $y$ axis. (c),(f) The gray surfaces are the complex spectrum as a function of $q_\parallel$ for the cases shown in (b),(e), respectively. The green, orange, and pink surfaces correspond to $q_\parallel = 0.5\pi$, $q_\parallel = 0$, and $q_\parallel = -0.6\pi$, respectively.

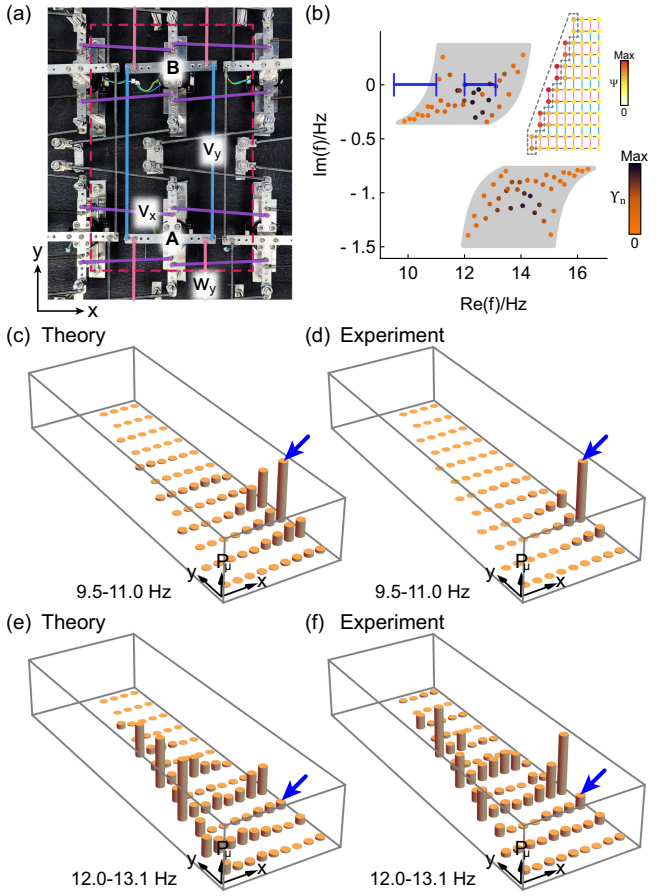


FIG. 3. (a) The photo of the coupled rotational oscillators realizing the unit cell shown in Fig. 1(a). (b) The OBC complex spectrum (colorful dots) of the trapezoidal structure with 78 sites. The gray background displays the corresponding PBC complex spectrum, and the color of the solid dots represents $\Upsilon_n$. Inset: the spatial distribution of $\Psi(\mathbf{x})$. The dashed line encloses the region $\mathscr{B}$. The plots of the (c),(e) theoretical and (d),(f) experimental spectral sum with different input chirp signals covering the frequency intervals (e),(f) $\Delta f_1 = [12.0, 13.1]$ and (c),(d) $\Delta f_2 = [9.5, 11.0]$ Hz. The blue arrows in (c)–(f) mark the source.

where $\omega_b \in \mathbb{C}$ is a reference energy. Note that Eq. (2) integrates over $q_\perp$ along $\Gamma_{q_\parallel}$, which is a closed loop [the solid blue line in Fig. 2(b), which is equivalent to the combination of the red dashed lines]. For any $q_\parallel$, if $\mathcal{W}_{q_\parallel} \neq 0$, which indicates that the spectral loop encloses a nonzero area, no two solutions of $q_\perp$ can be found at the same energy. Skin effects must occur. In contrast, if $\forall\, q_\parallel$ in BZ, $\mathcal{W}_{q_\parallel} = 0$, i.e., the spectral loops have no interior, so at each energy, the incident and reflected waves can have different $q_\perp$. As a result, the reflected channel exists at the boundary, and the skin effect is absent. In Fig. 2(c), we show the PBC spectrum as a function of $q_\parallel$ for the slanted edge. Spectral loops enclosing nonzero areas exist for most $q_\parallel$, e.g., at $q_\parallel = 0.5\pi$ and $q_\parallel = -0.6\pi$. Hence the skin effect occurs at this edge [Fig. 1(d)]. However, if the boundary cuts parallelly to the $y$ direction, as shown in Figs. 2(d)–2(f), the spectral loops collapse to arcs and enclose zero areas for all $q_\parallel$, so $\mathcal{W}_{q_\parallel}$ always vanishes [Fig. 2(f)]. Thus, the skin effect must be absent at this boundary [Fig. 1(c)].

To summarize, our system is both Lorentz and spectral reciprocity, which differs intrinsically from the nonreciprocal scenarios, and thereby the presence or absence of the skin effect only depends on the boundary orientation of the OBC lattice or, equivalently, the geometry of the OBC lattice. This feature makes the GDSE unique to higher-dimensional non-Hermitian systems. Moreover, it is worth pointing out that the superposition of quasi-1D spectra cannot reproduce the 2D OBC spectra, which emphasizes the necessity of considering the 2D nature of the lattice and highlights the role of dimensionality in non-Hermitian physics [41]. Besides demonstrating the uniqueness of the GDSE, we further show its wave function, including the exponential decay away from the boundary, the inverse participation ratio and robustness against onsite disorders, and the number of skin modes obeying the volume law, corroborating that the GDSE satisfies the required properties of the NHSE [41]. We remark that the onsite gain in our systems is essential for

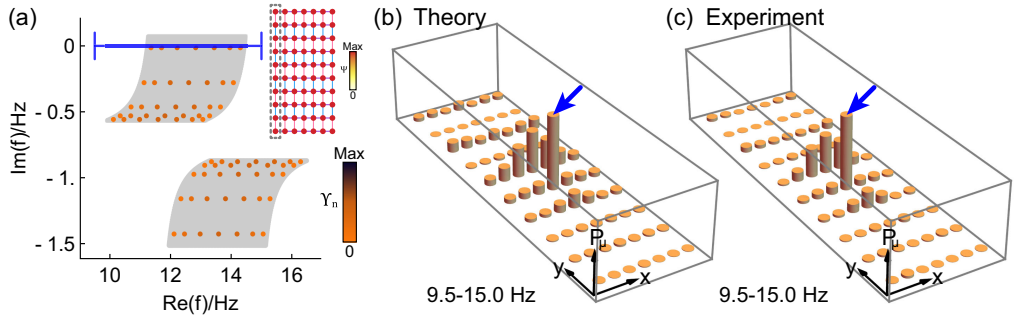


FIG. 4. (a) The OBC complex spectrum (colorful dots) of the rectangular structure with 70 sites. The color bar is the same as in Fig. 3(b). Inset: the spatial distribution of $\Psi(\mathbf{x})$. The gray dashed line encloses the region $\mathscr{B}$. The plots of the (b) theoretical and (c) experimental spectral sum with input chirp signal covering 9.5–15.0 Hz. The blue arrows in (b),(c) mark the source.

the direct observation of the GDSE. Because in loss-biased systems, eigenvalues have large negative imaginary parts, meaning that the temporal decay plays a significant role in the response measurements [41].

*Experimental realization.*—Equation (1) can be realized in an active mechanical lattice [36,45]. The unit cell consisting of two rotational oscillators coupled by tension springs is shown in Fig. 3(a). The non-Hermitian terms, i.e., onsite loss $(-i\gamma_A)$ and gain $(i\gamma_B)$, are achieved by imposing a self-feedback torque $\tau(t) = \beta\dot{\theta}(t)$ on every oscillator [41]. Here, $\dot{\theta}(t)$ is the instantaneous angular velocity and $\beta$ is a tunable constant. When $\beta$ is positive (negative), $\tau(t)$ acts as effective gain (loss). However, we found that the active torque also introduces a $\beta$-dependent perturbation to the onsite resonance (see Ref. [41] for details). This is accounted for by $f_A$ and $f_B$ in Eq. (1). All coefficients in Eq. (1) are obtained by Green's function from the measured data [16] (see Ref. [41] for the retrieved values).

Our first experimental system is a trapezoidal lattice consisting of $N = 78$ sites [Figs. 3(b) and S13 [41]]. The corresponding OBC complex spectrum, denoted $\omega^{\mathrm{O}}$, is shown in Fig. 3(b). To quantify the degree of localization of each mode, we introduce the quantity

$$\Upsilon_n = \frac{\sum_{\mathbf{x}\in\mathscr{B}} |\psi_n(\mathbf{x})|^2}{\sum_{\mathbf{x}} |\psi_n(\mathbf{x})|^2}, \tag{3}$$

where $\mathscr{B}$ denotes the slanted boundary region with the width of a single unit cell [indicated by the gray dashed line in the inset of Fig. 3(b)]. A large $\Upsilon_n$ indicates the corresponding wavefunction is strongly localized in $\mathscr{B}$. In Fig. 3(b), the color of the dots represents $\Upsilon_n$. Strongly localized modes are found near $\mathrm{Re}(\omega^{\mathrm{O}}/2\pi) \in (12.0, 13.1)$ Hz. These modes lie near $\mathrm{Im}(\omega^{\mathrm{O}}/2\pi) \cong 0$, so that they can be stably excited with minimal temporal decay. Experimentally, a source placed at the right edge sends a pulsing containing $\Delta f_1 = [12.0, 13.1]$ Hz. The spectral responses $A_u(f)$ are measured across the entire lattice, where $u$ denotes the site number. We then compute the spectral sum

$$P_u = \int_{\Delta f_1} |A_u(f)|^2 \mathrm{d}f. \tag{4}$$

The result shows a drop in $P_u$ immediately away from the source, but then it increases again and peaks at the slanted edge [Fig. 3(f)], which is strong evidence of the skin effect. No localization is observed at the boundaries parallel to the $x$ and $y$ directions. We also perform theoretical calculations of the spectral sum by solving the time-dependent Schrödinger equation [Fig. 3(e)]. Good agreement between them can be observed, thereby evidencing the GDSE, although the lattice size is not large. Note that the localization will become more pronounced if the lattice becomes larger [41].

In a control experiment, we excite the lattice at the same position but with a pulse containing $\Delta f_2 = [9.5, 11.0]$ Hz. The modes in this frequency interval have small $\Upsilon_n$, but their imaginary eigenfrequencies are negative $\mathrm{Im}(\omega^{\mathrm{O}}/2\pi) < 0$, which indicates a temporal decaying characteristic. Their responses are shown in Fig. 3(d), which indeed decay rapidly away from the source. These results, together with Fig. 3(f), conform well with the predictions of the GDSE and necessitate the onsite gain in the direct experimental observation of the GDSE. [The modes lying within $\mathrm{Re}(\omega^{\mathrm{O}}/2\pi) \in (11.0, 12.0) \cup (13.1, 14.1)$ Hz have $\mathrm{Im}(\omega^{\mathrm{O}}/2\pi) > 0$. They are temporally unstable and hence are not excited by purposely avoiding the corresponding frequencies].

For further validation, we perform similar experiments on the same system arranged in a rectangular lattice consisting of 70 sites [Figs. 4(a) and S14 [41]]. Figure 4(a) plots the PBC and OBC spectra. In the inset, $\Psi(\mathbf{x})$ is clearly uniform, which indicates the absence of the skin effect. The color of the OBC spectrum represents $\Upsilon_n$ with the region $\mathscr{B}$ now being the left edge. Compared with Fig. 3(b), all $\Upsilon_n$ are close to zero, which suggests that the modes are extended. In the experiment, the source is placed in the bulk, and the excitation covers 9.5–15.0 Hz. The spectral sum plotted in Fig. 4(c) shows the typical behavior of the bulk modes under dissipation, which is in good

agreement with the theoretical result [Fig. 4(b)]. No localization at the other boundaries occurs.

*Discussions.*—Interestingly, owing to the spectral reciprocity, when $q_{\parallel} = 0$, the condition $\omega^P(0, q_\perp) = \omega^P(0, -q_\perp)$ is always met. It follows that $\mathcal{W}_{q_{\parallel}=0} = 0$, as shown by the blue curve in Fig. 2(c). This implies that reflective channels always exist for the normal-incident waves, regardless of the orientation of the boundary $q_{\parallel}$. As a result, even when the GDSE occurs, a portion of modes must remain extended bulk modes, which would be clearly identified in the thermodynamic limit. In contrast, if spectral reciprocity breaks, then $\forall\, q_{\parallel}$ in the BZ, $\mathcal{W}_{q_{\parallel}} \neq 0$, so all modes are skin modes. (Exceptions such as the modes at the "Bloch points," which denote the cross points of two spectral loops with the opposite winding numbers [46], may exist, but those are not generic cases and usually require parameter tuning).

The GDSE is potentially useful for wave-localization applications. Compared to bound states localized at defects or boundaries, the wave localization from skin modes is naturally broadband in character. While compared to disorder-induced localization that can occur anywhere in a random medium, skin modes are deterministically boundary localized. On the other hand, the presence of gain implies that a portion of the skin modes can have positive imaginary parts, meaning that they are temporally divergent [41]. These modes, if realized in optical systems, are potential candidates for lasing.

In summary, we have demonstrated the GDSE in a 2D spectral and Lorentz reciprocal mechanical system in which the only non-Hermiticity is the gain and loss. The origin of the GDSE is an interplay of the PBC spectrum, lattice symmetry, and macroscopic symmetry of the lattice. In other words, the skin effect occurs in generic geometric shapes as long as the macroscopic geometry does not align with any lattice symmetries. Equivalently, the persistence of extended bulk modes against the non-Hermiticity requires the combined protection of the reciprocity and the lattice symmetries. Therefore, our results not only reveal the universality of the skin effect in systems with dimensions higher than one but also highlight the vital role of macroscopic geometry and symmetry for the skin effects. Recent works have also predicted that the interplay between geometry and symmetry can dramatically alter the generalized BZ of 2D systems, including its shapes and even dimensionality [42,43,47].

*Note added.*— Recently, we became aware of two works reporting the GDSE in acoustic systems. See Refs. [48,49].

This work is supported by the National Key R&D Program of China (No. 2022YFA1404500, No. 2022YFA1404400, No. 2022YFA1404701), the National Natural Science Foundation of China (No. 12174072, No. 11922416, No. 2021hwyq05), the Hong Kong Research Grants Council (No. RFS2223-2S01, No. 12302420, No. 12300419, No. 12301822), the China Postdoctoral Science Foundation (No. 2023M730705), and the Natural Science Foundation of Shanghai (No. 21ZR1403700).

[*] These authors contributed equally.

[1] C. M. Bender and S. Boettcher, Real spectra in Non-Hermitian Hamiltonians having $P\ T$ symmetry, Phys. Rev. Lett. **80**, 5243 (1998).
[2] C. M. Bender, D. C. Brody, and H. F. Jones, Complex extension of quantum mechanics, Phys. Rev. Lett. **89**, 270401 (2002).
[3] C. M. Bender, Making sense of non-Hermitian Hamiltonians, Rep. Prog. Phys. **70**, 947 (2007).
[4] I. Rotter, A Non-Hermitian Hamilton operator and the physics of open quantum systems, J. Phys. A **42**, 153001 (2009).
[5] Y. Ashida, Z. Gong, and M. Ueda, Non-Hermitian physics, Adv. Phys. **69**, 249 (2020).
[6] M. Z. Hasan and C. L. Kane, Colloquium: Topological insulators, Rev. Mod. Phys. **82**, 3045 (2010).
[7] E. J. Bergholtz, J. C. Budich, and F. K. Kunst, Exceptional topology of non-Hermitian systems, Rev. Mod. Phys. **93**, 015005 (2021).
[8] K. Ding, C. Fang, and G. Ma, Non-Hermitian topology and exceptional-point geometries, Nat. Rev. Phys. **4**, 745 (2022).
[9] N. P. Armitage, E. J. Mele, and A. Vishwanath, Weyl and Dirac semimetals in three-dimensional solids, Rev. Mod. Phys. **90**, 015001 (2018).
[10] Z. Gong, Y. Ashida, K. Kawabata, K. Takasan, S. Higashikawa, and M. Ueda, Topological phases of non-Hermitian systems, Phys. Rev. X **8**, 031079 (2018).
[11] H. Shen, B. Zhen, and L. Fu, Topological band theory for Non-Hermitian Hamiltonians, Phys. Rev. Lett. **120**, 146402 (2018).
[12] K. Kawabata, T. Bessho, and M. Sato, Classification of exceptional points and non-Hermitian topological semimetals, Phys. Rev. Lett. **123**, 066405 (2019).
[13] K. Kawabata, K. Shiozaki, M. Ueda, and M. Sato, Symmetry and topology in non-Hermitian physics, Phys. Rev. X **9**, 041015 (2019).
[14] C. Dembowski, H.-D. Gräf, H. L. Harney, A. Heine, W. D. Heiss, H. Rehfeld, and A. Richter, Experimental observation of the topological structure of exceptional points, Phys. Rev. Lett. **86**, 787 (2001).
[15] C. E. Rüter, K. G. Makris, R. El-Ganainy, D. N. Christodoulides, M. Segev, and D. Kip, Observation of parity–time symmetry in optics, Nat. Phys. **6**, 192 (2010).
[16] K. Ding, G. Ma, M. Xiao, Z. Q. Zhang, and C. T. Chan, Emergence, coalescence, and topological properties of multiple exceptional points and their experimental realization, Phys. Rev. X **6**, 021007 (2016).
[17] B. Zhen, C. W. Hsu, Y. Igarashi, L. Lu, I. Kaminer, A. Pick, S.-L. Chua, J. D. Joannopoulos, and M. Soljačić, Spawning rings of exceptional points out of Dirac cones, Nature (London) **525**, 354 (2015).

[18] A. Cerjan, S. Huang, M. Wang, K. P. Chen, Y. Chong, and M. C. Rechtsman, Experimental realization of a Weyl exceptional ring, Nat. Photonics **13**, 623 (2019).
[19] W. Tang, X. Jiang, K. Ding, Y.-X. Xiao, Z.-Q. Zhang, C. T. Chan, and G. Ma, Exceptional nexus with a hybrid topological invariant, Science **370**, 1077 (2020).
[20] J. Liu, Z. Li, Z.-G. Chen, W. Tang, A. Chen, B. Liang, G. Ma, and J.-C. Cheng, Experimental realization of Weyl exceptional rings in a synthetic three-dimensional non-Hermitian phononic crystal, Phys. Rev. Lett. **129**, 084301 (2022).
[21] L. Feng, R. El-Ganainy, and L. Ge, Non-Hermitian photonics based on parity–time symmetry, Nat. Photonics **11**, 752 (2017).
[22] M.-A. Miri and A. Alù, Exceptional points in optics and photonics, Science **363**, eaar7709 (2019).
[23] Ş. K. Özdemir, S. Rotter, F. Nori, and L. Yang, Parity–time symmetry and exceptional points in photonics, Nat. Mater. **18**, 783 (2019).
[24] S. Yao and Z. Wang, Edge states and topological invariants of non-Hermitian systems, Phys. Rev. Lett. **121**, 086803 (2018).
[25] F. K. Kunst, E. Edvardsson, J. C. Budich, and E. J. Bergholtz, Biorthogonal bulk-boundary correspondence in non-Hermitian systems, Phys. Rev. Lett. **121**, 026808 (2018).
[26] D. S. Borgnia, A. J. Kruchkov, and R.-J. Slager, Non-Hermitian boundary modes and topology, Phys. Rev. Lett. **124**, 056802 (2020).
[27] K. Zhang, Z. Yang, and C. Fang, Correspondence between winding numbers and skin modes in non-Hermitian systems, Phys. Rev. Lett. **125**, 126402 (2020).
[28] N. Okuma, K. Kawabata, K. Shiozaki, and M. Sato, Topological origin of non-Hermitian skin effects, Phys. Rev. Lett. **124**, 086801 (2020).
[29] X. Zhang, T. Zhang, M.-H. Lu, and Y.-F. Chen, A review on non-Hermitian skin effect, Adv. Phys. X **7**, 2109431 (2022).
[30] T. E. Lee, Anomalous edge state in a non-Hermitian lattice, Phys. Rev. Lett. **116**, 133903 (2016).
[31] S. Weidemann, M. Kremer, T. Helbig, T. Hofmann, A. Stegmaier, M. Greiter, R. Thomale, and A. Szameit, Topological funneling of light, Science **368**, 311 (2020).
[32] L. Xiao, T. Deng, K. Wang, G. Zhu, Z. Wang, W. Yi, and P. Xue, Non-Hermitian bulk–boundary correspondence in quantum dynamics, Nat. Phys. **16**, 761 (2020).
[33] A. Ghatak, M. Brandenbourger, J. van Wezel, and C. Coulais, Observation of non-Hermitian topology and its bulk–edge correspondence in an active mechanical metamaterial, Proc. Natl. Acad. Sci. U.S.A. **117**, 29561 (2020).
[34] L. Zhang *et al.*, Acoustic non-Hermitian skin effect from twisted winding topology, Nat. Commun. **12**, 6297 (2021).
[35] D. Zou, T. Chen, W. He, J. Bao, C. H. Lee, H. Sun, and X. Zhang, Observation of hybrid higher-order skin-topological effect in non-Hermitian topolectrical circuits, Nat. Commun. **12**, 7201 (2021).
[36] W. Wang, X. Wang, and G. Ma, Non-Hermitian morphing of topological modes, Nature (London) **608**, 50 (2022).
[37] Y. Yi and Z. Yang, Non-Hermitian skin modes induced by on-site dissipations and chiral tunneling effect, Phys. Rev. Lett. **125**, 186802 (2020).
[38] K. Zhang, Z. Yang, and C. Fang, Universal non-Hermitian skin effect in two and higher dimensions, Nat. Commun. **13**, 2496 (2022).
[39] T. Hofmann *et al.*, Reciprocal skin effect and its realization in a topolectrical circuit, Phys. Rev. Res. **2**, 023265 (2020).
[40] Z. Fang, M. Hu, L. Zhou, and K. Ding, Geometry-dependent skin effects in reciprocal photonic crystals, Nanophotonics **11**, 3447 (2022).
[41] See Supplemental Material at http://link.aps.org/supplemental/10.1103/PhysRevLett.131.207201 for detailed discussions on various properties of the GDSE, the experimental setup, and potential applications, which includes Refs. [38,42–44].
[42] H. Jiang and C. H. Lee, Dimensional transmutation from non-hermiticity, Phys. Rev. Lett. **131**, 076401 (2023).
[43] H.-Y. Wang, F. Song, and Z. Wang, Amoeba formulation of the non-Hermitian skin effect in higher dimensions, arXiv:2212.11743.
[44] T. Liu, Y.-R. Zhang, Q. Ai, Z. Gong, K. Kawabata, M. Ueda, and F. Nori, Second-order topological phases in non-hermitian systems, Phys. Rev. Lett. **122**, 076801 (2019).
[45] W. Wang, X. Wang, and G. Ma, Extended state in a localized continuum, Phys. Rev. Lett. **129**, 264301 (2022).
[46] F. Song, S. Yao, and Z. Wang, Non-Hermitian topological invariants in real space, Phys. Rev. Lett. **123**, 246801 (2019).
[47] K. Yokomizo and S. Murakami, Non-Bloch bands in two-dimensional non-Hermitian systems, Phys. Rev. B **107**, 195112 (2023).
[48] Q. Zhou, J. Wu, Z. Pu, J. Lu, X. Huang, W. Deng, M. Ke, and Z. Liu, Observation of geometry-dependent skin effect in non-Hermitian phononic crystals with exceptional points, Nat. Commun. **14**, 4569 (2023).
[49] T. Wan, K. Zhang, J. Li, Z. Yang, and Z. Yang, Observation of the geometry-dependent skin effect and dynamical degeneracy splitting, Sci. Bull. **68**, 2330 (2023).